Rendering Polyurethane Hydrophilic for Efficient Cellulose Reinforcement in Melt-Spun Nanocomposite Fibers

Alexandre Redondo, Livia K. Bast, Kenza Djeghdi, Martino Airoldi, Daseul Jang, LaShanda T. J. Korley, Ullrich Steiner,* Nico Bruns,* and Ilja Gunkel*

Many commodity plastics, such as thermoplastic polyurethanes (PUs), require reinforcement for use as commercial products. Cellulose nanocrystals (CNCs) offer a "green" and scalable approach to polymer reinforcement as they are exceptionally stiff, recyclable, and abundant. Unfortunately, achieving efficient CNC reinforcement of PUs with industrial melt processing techniques is difficult, mostly due to the incompatibility of the hydrophobic PU with hydrophilic CNCs, limiting their dispersion. Here, a hydrophilic PU is synthesized to achieve strong reinforcement in melt-processed nanocomposite fibers using filter paper-sourced CNCs. The melt-spun fibers, exhibiting smooth surfaces even at high CNC loading (up to 25 wt%) indicating good CNC dispersion, are bench-marked against solvent-cast films—solvent processing is not scalable but disperses CNCs well and produces strong CNC reinforcement. Mechanical analysis shows the CNC addition stiffens both nanocomposite films and fibers. The stress and strain at break, however, are not significantly affected in films, whereas adding CNCs to fibers increases the stress-at-break while reducing the strain-at-break. Compared to earlier studies employing a hydrophobic (and stiffer) PU, CNC addition to a hydrophilic PU substantially increases the fiber stiffness and strength. This work therefore suggests that rendering thermoplastics more hydrophilic might pave the way for "greener" polymer composite products using CNCs.

1. Introduction

Nano-sized cellulose[1] holds promise for sustainable development of high-performance composite materials.[2] Cellulose nanocrystals (CNCs), for example, are not only exceptionally

stiff but also biocompatible, biodegradable, recyclable, and hugely abundant.[3] These rod-shaped nanocrystals have a stiffness similar to Kevlar,[4] which makes them ideal candidates for fabricating reinforced polymer nanocomposites.[5] Despite increasing research efforts, CNC reinforcement is not yet applicable to commercial polymer products.[6] Generally, the incompatibility between the inherently hydrophilic CNCs and the mostly hydrophobic commodity plastics is still challenging, as is the integration of CNCs into common industrial processing.

Among the various commodity plastics, polyurethanes (PUs) are particularly interesting candidates for cellulose reinforcement. They are used in a broad range of industrial applications due to their outstanding mechanical properties and versatility.[7] Thermoplastic PUs, for example, find use in the automotive industry as they are tough, flexible, and resistant to abrasion, but they lack mechanical strength and are therefore commonly reinforced with carbon fibers.[8] Aiming at "green" reinforcement alternatives, recent research on PU and other polymer nanocomposites instead focused on CNCs with the specific goal of achieving efficient reinforcement using industrially relevant melt processing techniques.[6]

There are currently only few examples of CNC/PU nanocomposites produced by melt processing,[9–12] or other

A. Redondo, L. K. Bast,† K. Djeghdi, M. Airoldi, U. Steiner, I. Gunkel
Adolphe Merkle Institute
University of Fribourg
Chemin des Verdiers 4, 1700 Fribourg, Switzerland
E-mail: ilja.gunkel@unifr.ch; ullrich.steiner@unifr.ch

The ORCID identification number(s) for the author(s) of this article can be found under https://doi.org/10.1002/admi.202201979.

[†]The author deceased on July 10, 2021

L. K. Bast, N. Bruns
Department of Pure and Applied Chemistry
University of Strathclyde
Thomas Graham Building, 295 Cathedral Street, Glasgow G1 1XL, UK

D. Jang, L. T. J. Korley
Departments of Materials Science & Engineering
and Chemical & Biomolecular Engineering
University of Delaware
Newark, DE 19716, USA

N. Bruns
Department of Chemistry
Technical University of Darmstadt
Alarich-Weiss-Str. 4, 64287 Darmstadt, Germany
E-mail: nico.bruns@tu-darmstadt.de
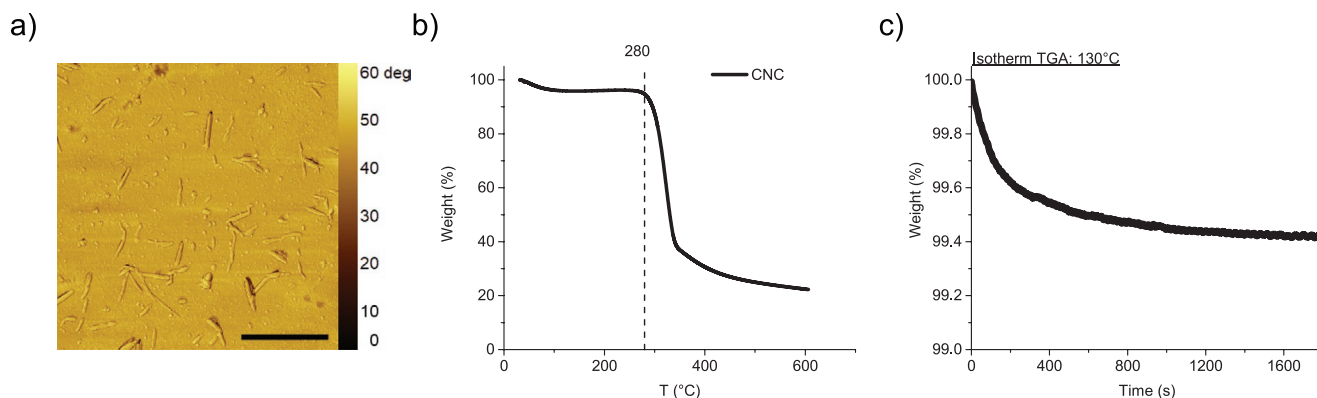
Figure 1. a) Atomic force microscopy (AFM) phase image of cotton CNCs. Scale bar: 1 μm b) Thermogravimetric analysis (TGA) of the CNCs with an onset temperature for degradation of 280 °C. c) Isotherm TGA of the CNCs measured at 130 °C for 30 min.

solvent-free processing techniques.[13] For melt mixing, the thermal stability of CNCs at the typical processing temperatures of thermoplastic PUs (180–210 °C)[9,10,12] is ensured by using phosphoric acid hydrolysis to isolate CNCs from cellulose. Compared to sulfuric acid hydrolysis, CNC extraction using phosphoric acid reduces the charge density on the surface of the CNCs and improves their thermal stability.[14] Achieving good CNC dispersion in melt-processed PU nanocomposites, however, remains a problem. While dispersion can be improved by initial solvent casting[15] or functionalization of the CNC surface,[11] these approaches are difficult to scale up and often the CNC loading and the extent of reinforcement remain limited. The mostly subpar reinforcement in melt-processed nanocomposites becomes particularly clear when fibers are directly compared to solvent-processed films: while melt-processed CNC/PU fibers outperform films at rather low CNC concentrations—especially for high-aspect ratio CNCs, sourced from prohibitively scarce tunicates[10]—films are superior at higher CNC concentrations.[12] The different mechanical performance of nanocomposite films and fibers is partly due to their distinct reinforcement mechanisms. While CNCs form a stiff network through a CNC-CNC hydrogen bonding network enabled by their isotropic orientation in films upon solvent processing, reinforcement in melt-processed fibers mostly stems from longitudinal CNCs alignment,[12] where they show maximum stiffness.[16] In theory, the maximum reinforcement in fibers is dictated by the aspect ratio of the CNCs and is optimized through their alignment. In practice, however, melt-processed nanocomposite fibers often show lower degrees of CNC dispersion than their solution-processed counterparts, which inhibits effective stress transfer from the matrix to the CNCs, thereby limiting reinforcement.[2] This limited dispersion is not observed when polar polymers, such as poly(vinyl alcohol),[17,18] poly(ethylene glycol),[19] or poly(hydroxybutyrate)[20] are used either directly as matrix for the CNCs or as dispersing agents due to their favorable interfacial interactions with the hydrophilic CNCs. Introducing strong polar groups into thermoplastic PUs is expected to similarly improve CNC dispersion in melt-processed CNC/PU fibers.

In this work, a hydrophilic and comparably soft polyurethane was synthesized to maximize the CNC/PU interfacial interactions and to facilitate melt processing with the ultimate goal of achieving efficient reinforcement. Cotton CNCs from commercially available filter paper were rendered thermally stable by phosphoric acid hydrolysis before using them as reinforcement agent. The degree of CNC alignment in melt-spun nanocomposite fibers was evaluated using wide-angle X-ray scattering (WAXS). Using tensile testing, the mechanical properties of melt-spun CNC/PU nanocomposite fibers with CNC-concentrations up to 25 wt% were assessed and compared with those of solvent-cast nanocomposites films in the context of standard semi-empirical reinforcement models.

2. Results and Discussion

2.1. Cellulose Nanocrystal Characterization

Cellulose sourced from filter paper was hydrolyzed using an adapted version of the phosphoric acid hydrolysis described by Camarero Espinosa et al.,[14] yielding CNCs with an average length of 85 ± 25 nm and an average thickness of 7 ± 2 nm as obtained from analyzing atomic force microscopy (AFM) images of the CNCs (**Figure 1**a).[12] These CNCs were previously shown to have a crystallinity ≈80%, which is similar to the crystallinity obtained after sulfuric acid hydrolysis.[14] The CNCs used here exhibit a high thermal stability with an onset of degradation at a temperature of 280 °C (Figure 1b). The thermal stability of the CNCs at the extrusion temperature of the polymer was measured with an isothermal thermogravimetric analysis (TGA) at 130 °C for 30 min during which no significant change of mass (mass reduction <1%) was detected, indicating the absence of CNC degradation within this time (Figure 1c). This high thermal stability is also supported by visual inspection of the CNCs, which maintained their initial white color throughout the temperature treatment.

2.2. Synthesis of Hydrophilic PU; Melt Spinning of CNC/Hydrophilic PU Fibers; Fiber Morphology

To achieve favorable interactions between the PU matrix and the CNCs that enable high CNC loading into PU fibers, a hydrophilic PU (HPU) was synthesized (**Figure 2**) by adapting
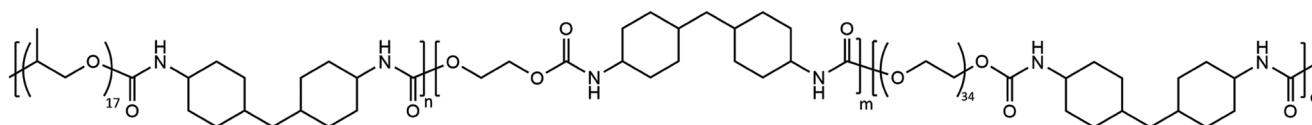
Figure 2. Chemical structure of hydrophilic PU (HPU) with poly(ethylene glycol) (PEG) linkers in the backbone rendering the polymer hydrophilic.

a previously reported synthesis protocol,[21–23] (Figure S1, Supporting Information) which introduces poly(ethylene glycol) (PEG) linkers into the backbone of the PU. The hydrophilic nature of HPU was confirmed by water uptakes of about 30 wt%. The protocol was extended by a thermal post-polymerization treatment of the HPU, which increased its molecular weight through an allophanate formation with an excess of the diisocynate Desmodur W (Figure S2, Supporting Information). For the melt-spinning of CNC/HPU nanocomposites, a masterbatch approach was employed, similar to an earlier approach that yielded nanocomposite HPU fibers with a CNC content of up to 20%.[12] To this end, the CNCs were dispersed in a solution of the PU and solvent-cast prior to melt-processing. This nanocomposite was fed into an extruder with synthesized neat PU samples to achieve the desired CNC concentration. The elasticity of the HPU and the compatibility of hydrophilic CNCs with this hydrophilic matrix allowed the processing of fibers nanocomposites with CNC concentrations as high as 25 wt%, without spin-failure. **Figure 3** shows fibers with very smooth surfaces for all CNC concentrations and the absence of any CNC aggregation, demonstrating the efficient dispersion and good compatibility of the CNCs with the hydrophilic matrix. This is in contrast to previous work on non-hydrophilic PU where the addition of 1 wt% CNCs into the PU matrix already significantly roughened the fiber surface.[10,12]

To minimize any effect of the fiber diameter on the mechanical properties, the drawing process was carefully controlled to achieve similar fibers diameters for all CNC concentrations. The produced fibers were 270–300 μm in diameter (**Table 1**).

2.3. CNC Orientation

Similar to earlier studies,[10,12] the CNCs in the CNC/HPU nanocomposite fibers were aligned by melt spinning and drawing. The WAXS profiles of the CNC/HPU nanocomposites in **Figure 4** show a broad single reflection arising from the HPU matrix and multiple reflections stemming from the CNCs. Note that the CNC signal exhibits two or four intense arc-shaped reflections in a similar q-range as the HPU reflection. The segmented nature of the CNC reflections indicates a preferential alignment of the CNCs within the materials. The solvent-cast CNC/HPU nanocomposite films, on the other hand, display isotropic reflections, indicating the absence of a preferential CNC orientation.

To further analyze the degree of orientation, azimuthal integration of the 2D WAXS profiles was performed. **Figure 5** shows the integrated fiber and film nanocomposite profiles, each of which features an intense and broad reflection at $q = 1.38$ Å^{-1}. Similar amorphous reflections (at slightly higher q values) are observed for commercial PU.[12] This absence of any significant crystallinity is also consistent with the differential scanning calorimetry (DSC) (Figure S7, Supporting Information). The observed CNC peaks overlap with this broad HPU reflection. The CNC peaks
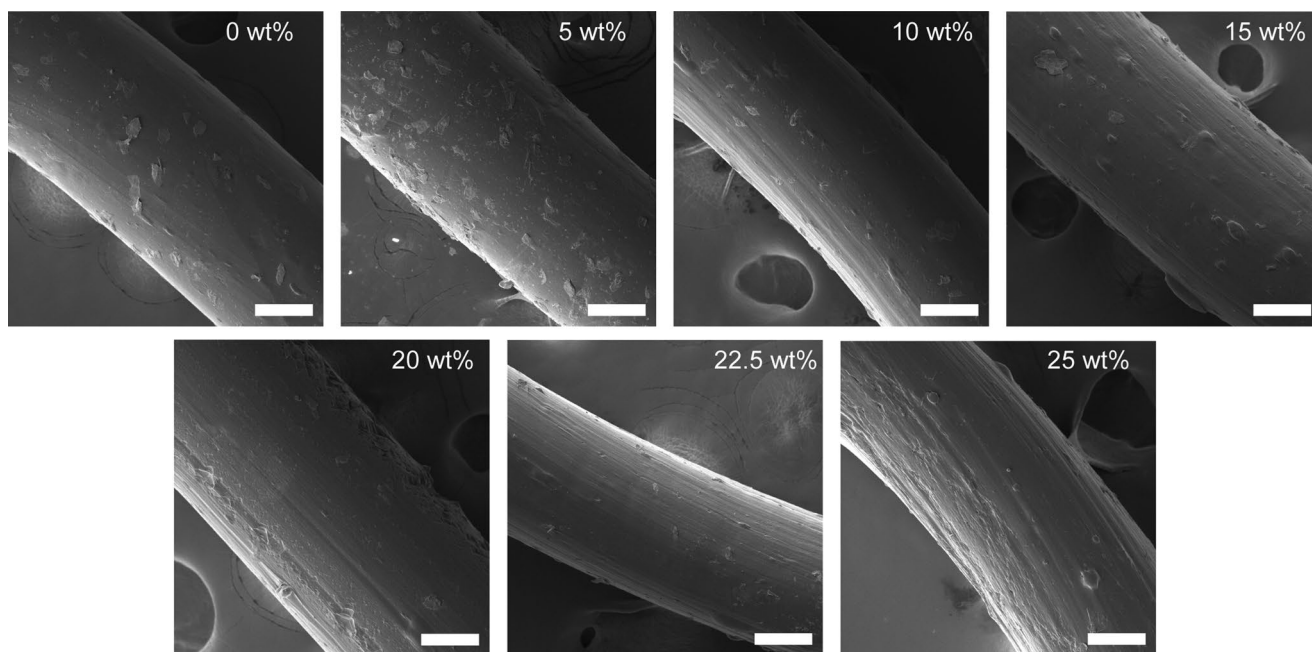
Figure 3. Scanning electron microscopy (SEM) images of CNC/HPU fiber nanocomposites showing smoothness of the fibers up to high CNC concentrations. All scale bars represent 100 μm.

ADVANCED
SCIENCE NEWS
www.advancedsciencenews.com

ADVANCED
MATERIALS
INTERFACES
www.advmatinterfaces.de

Table 1. Melt-spun fiber diameter, which was kept uniform for all CNC concentrations by adapting the spinning line conditions.

CNC concentration [wt%]	0	5	10	15	20	22.5	25
Fiber diameter [µm]	272 ± 15	298 ± 23	285 ± 25	281 ± 15	272 ± 5	270 ± 60	280 ± 76

at q values of 1.08 Å^{-1}, 1.2 Å^{-1}, 1.6 Å^{-1}, and 2.4 Å^{-1} correspond to the [1$\bar{1}$0], [110], [200], and the [004] reflections, respectively. The CNC peak intensities increase with concentration.

The azimuthal nanocomposite fiber and film profiles at $q = 1.6 \pm 0.05$ Å^{-1} and $q = 2.4 \pm 0.05$ Å^{-1} are also shown in Figure 5. The azimuthal profile of nanocomposite films in Figure 5b–d confirm their isotropic nature. Note that both PU and CNC reflections present essentially flat azimuthal profiles at all concentrations in the nanocomposite CNC/HPU films. In contrast, the azimuthal profiles of nanocomposite fibers show the presence of intense peaks for both PU and CNCs reflections, indicating their anisotropic nature. To quantify the degree of orientation in the fibers, the Hermans orientation parameter was calculated based on the azimuthal profiles of both the CNC and the HPU reflections. The Hermans orientation parameter varies between 0 and 1, where values of 0 and 1 represent perfectly isotropic and aligned materials, respectively. The Hermans orientation parameters in **Table 2** show that CNC/HPU nanocomposite fibers exhibit a strong preferential orientation of the CNCs within the HPU matrix, yielding values of the Hermans orientation parameter ≈0.9. The degree of CNC alignment in HPU is significantly improved compared to the earlier study of ref. [12], where identically prepared and sourced CNCs were added to a non-hydrophilic (commercial) PU matrix with a maximum value of Hermans orientation parameter for CNCs of 0.74. Related to the improved CNC alignment, the matrix polymer in nanocomposite CNC/HPU fibers is also aligned, with a stronger alignment at higher CNC concentrations (Table 2), whereas the alignment of the matrix polymer in CNC/PU nanocomposite fibers deteriorated as the CNC load increased.[12] This high degree of alignment of both HPU and CNCs indicates beneficial CNC-HPU interactions as well as homogeneous CNC dispersion within the HPU matrix.
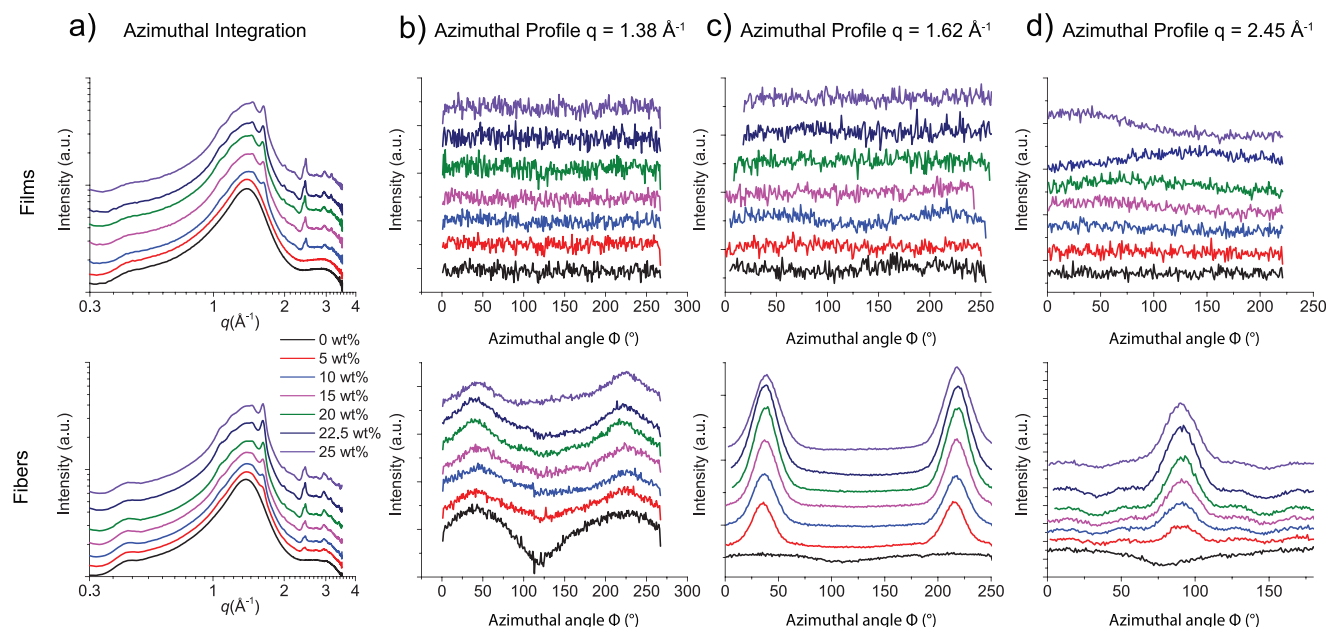
2.4. Mechanical Properties

To assess the extent of CNC reinforcement in CNC/HPU nanocomposite fibers, their mechanical properties were compared to those of solvent-processed CNC/HPU nanocomposite films based on tensile testing. **Figure 6**a,c shows the variation of Young's modulus with CNC content in melt-spun fibers. The addition of CNCs increases the stress-at-break of the fibers indirectly by facilitating the alignment of the polymeric matrix. The dependence of the stress-at-break on the polymer molecular orientation was reported previously.[10,12] The strain-at-break, however, decreases with CNC concentration as the high crystallinity of the CNCs decreases the ductility of the nanocomposite. Nevertheless, fiber nanocomposites containing 25 wt% CNCs retain a strain-at-break above 200%. The stress–strain curves of CNC/HPU film and fiber nanocomposites in Figure 6 differ strongly. In nanocomposite films, the strain-at-break and the stress-at-break are not significantly impacted by the addition of CNCs.

Both film and fiber Young's moduli increase with CNC addition, as shown in Figure 6. Neat PU fibers and films have Young's moduli of 5.4 and 4.5 MPa, respectively. With the addition of 25 wt% CNCs, both the fiber and film stiffness increases to 51.2 and 94.7 MPa, respectively. Note that the degree of reinforcement is larger in nanocomposite films, which is related to the low aspect ratio of the cotton CNCs used here, whose percolation in films provides stronger reinforcement than their alignment in nanocomposite fibers.[12]

It is interesting to compare the results of Figure 6 to the aforementioned earlier study of ref. [12], where identically prepared and sourced CNCs were added to a stiffer, non-hydrophilic PU matrix with Young's moduli of 21 and 11 MPa, for neat fibers and films, respectively. While the relative offset
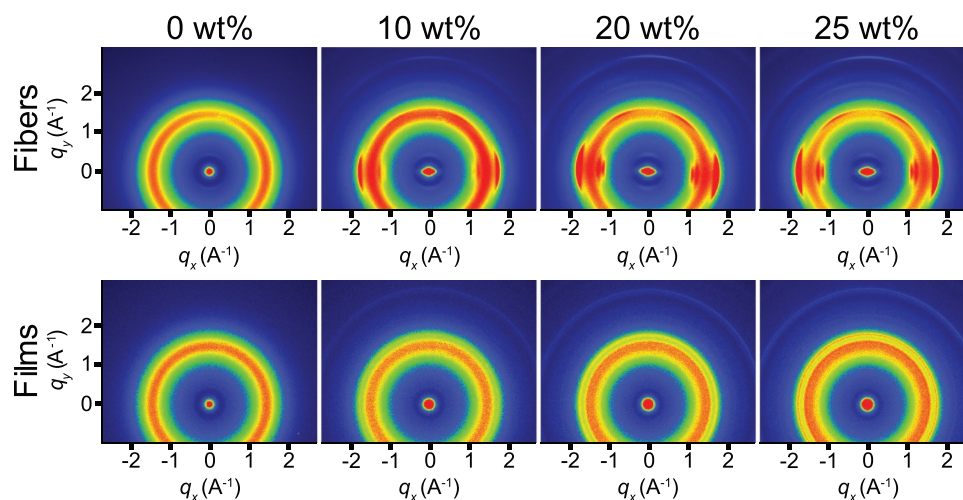
Figure 4. 2D WAXS patterns of CNC/HPU fiber and film nanocomposites. The patterns of the fibers display pronounced arc-shaped CNC reflections indicating a preferred alignment of the CNCs. All films present isotropic reflections.

ADVANCED
SCIENCE NEWS
www.advancedsciencenews.com

ADVANCED
MATERIALS
INTERFACES
Open Access
www.advmatinterfaces.de

Figure 5. a) Azimuthal integration of the WAXS profiles of Figure 4 for CNC/HPU film and fiber nanocomposites. Note the progressive increase in CNC reflections upon their addition. b) Azimuthal profiles of film and fiber nanocomposites of the PU main reflection at $q = 1.38$ Å^{-1}. c) CNC reflections at $q = 1.62$ Å^{-1} and d) $q = 2.45$ Å^{-1}.

in Young's moduli is preserved in the nanocomposite films (Figure 6), the stiffening of the nanocomposite fibers with increasing CNC concentration is much more pronounced in the case of the softer HPU matrix compared to the stiffer, non-hydrophilic PU. This larger extent of reinforcement in the softer HPU is evident as its Young's modulus nearly converges with that of the stiffer non-hydrophilic PU for the highest CNC contents. In addition, the stress–strain curves of the samples with the highest CNC content are very similar for both PU matrices. For the softer, hydrophilic matrix, the stress-at-break of the nanocomposite fibers is substantially increased upon CNC addition, while it is reduced in the case of the stiffer non-hydrophilic PU matrix.

The stiffness of the materials were compared to the Halpin–Tsai (HT) and percolation models to elucidate the reinforcement mechanism in the produced nanocomposites. The value of the parameters used are listed in **Table 3**. Figure 6c shows a

Table 2. Hermans orientation parameter of CNC/HPU fiber nanocomposites calculated for the PU reflection ($q = 1.38$ Å^{-1}) and for the CNC [200] and [004] reflections ($q = 1.62$ Å^{-1} and $q = 2.45$ Å^{-1}).

	Hermans order parameter		
CNC	$q = 1.38$ Å^{-1}	$q = 1.62$ Å^{-1}	$q = 2.45$ Å^{-1}
0 wt%	0.11	–	–
5 wt%	0.46	0.94	0.91
10 wt%	0.43	0.92	0.9
15 wt%	0.55	0.92	0.9
20 wt%	0.67	0.92	0.9
22.5 wt%	0.67	0.91	0.89
25 wt%	0.71	0.91	0.87

good match of the fibers' mechanical properties with the prediction of the HT model for unidirectionally aligned CNCs (see Experimental Section). Note this is in contrast to the behavior seen in hydrophobic PU, which was found to match the prediction of the isotropic HT model.[12] This difference between the reinforcement mechanisms at play in hydrophobic PU and HPU is associated with the higher degree of CNC alignment seen in HPU (Table 2) compared to hydrophobic PU. Moreover, the agreement between the experimental data of the CNC/HPU fibers with the HT model for unidirectionally aligned CNCs not only confirms the high degree of CNC alignment observed in the WAXS analysis (Table 2) but also suggest beneficial interactions between the CNCs and the HPU matrix as well as a homogeneous dispersion of CNCs within the hydrophilic matrix as these are two main assumptions of the HT model (see Experimental Section). On the other hand, the mechanical properties of the films match the percolation model (see Experimental Section). This finding implies that the CNCs in the nanocomposite films assemble into a rigid network, allowing the determination of Young's modulus of the CNCs of $E_n = 0.91$ GPa, based on a least-square fit. While the CNC concentration in composite films affects the stress–strain behavior only slightly, the CNC percolation stiffens films more substantially than the HT mechanism in fibers.

We speculate that the improved CNC reinforcement of a hydrophilic PU matrix is likely due to its more favorable interactions with the hydrophilic CNCs, allowing good CNC dispersion and efficient stress-transfer between the CNCs and the matrix. Such improved dispersion of the CNCs in the HPU matrix is consistent with the smooth surfaces of the nanocomposite fibers observed by SEM (Figure 3), which are rougher for fibers using a less hydrophilic PU matrix, especially at high CNC loading.[12] The favorable interactions between HPU and
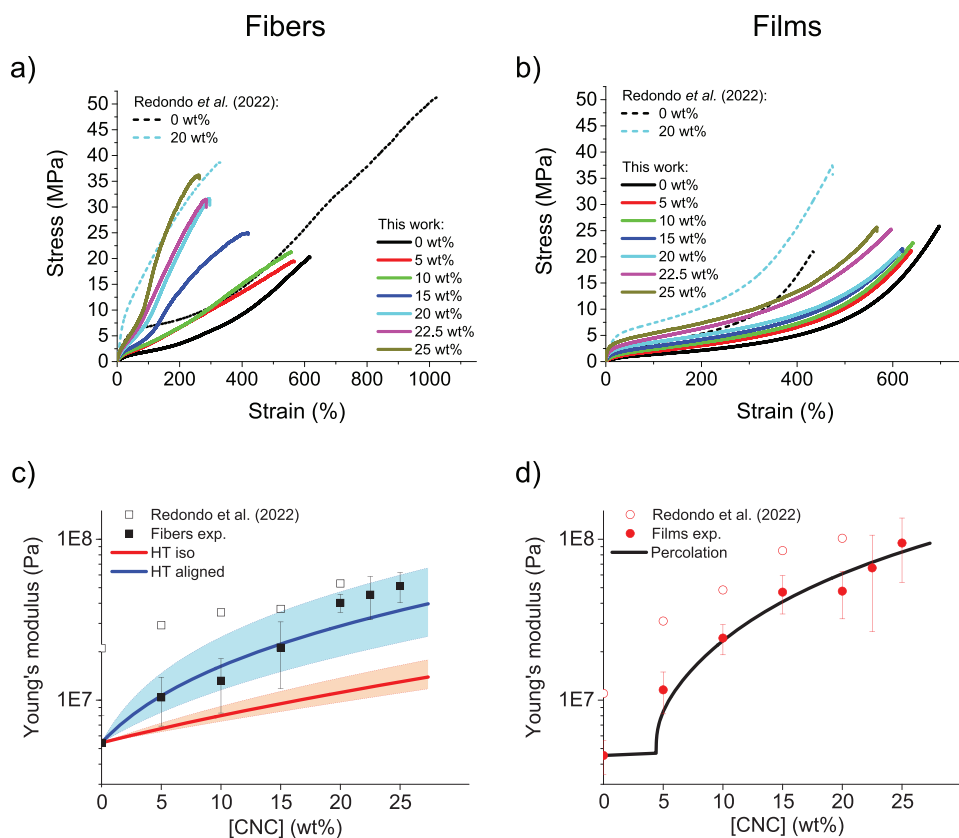
Figure 6. a) Mechanical properties of CNC/HPU fiber nanocomposites. The addition of CNCs increases both the Young's modulus and the stress-at-break, while reducing the strain-at-break, because of the stiffening of the nanocomposites by the CNCs. b) CNC/HPU film nanocomposite mechanical properties. The strain-at-break and stress-at-break are little affected by the addition of CNCs, whereas a strong stiffness reinforcement is observed. c) Fiber Young's modulus experimental data compared with two different HT models. Note that HT iso and HT aligned stand for the HT model for isotropically distributed CNCs and for unidirectionally aligned CNCs, respectively. The fiber mechanical properties are in agreement with the prediction of the HT model for unidirectionally aligned CNCs. d) Film Young's modulus experimental data compared with the percolation model. The results of ref. [12], where similar CNCs were studied in a stiffer, non-hydrophilic PU matrix are shown for comparison in c) and d).

the CNCs are also reflected in the strong preferred orientation of both CNCs as well as the HPU matrix in the nanocomposite fibers (Figure 5 and Table 2), which is less pronounced when a less hydrophilic and stiffer PU is used.[12]

3. Conclusion

This study investigates the reinforcement of melt-processed nanocomposite fibers made of a hydrophilic and low-elastic modulus PU matrix reinforced with cotton CNCs sourced from commercial filter papers. The high thermal stability of CNCs generated by phosphoric acid hydrolysis combined with a master-batch melt-spinning approach employing a comparably soft and hydrophilic PU matrix allowed the manufacture of

Table 3. Parameter values used in the models in Figure 6.

E_m	Matrix Young's modulus	4.5 MPa (films)/5.4 MPa (fibers)
E_n	Filler Young's modulus (films)	0.91 GPa
E_f	Filler Young's modulus (fibers)	78 GPa [24]
L/D	Filler aspect ratio	12.1

fibers with a CNC content of up to 25 wt%. Smooth fiber surfaces were observed at all CNC concentrations, which indicates that the hydrophilic character of the synthesized HPU allows for good dispersion of the (hydrophilic) CNCs, which is otherwise difficult to achieve in melt-processed nanocomposites using more hydrophobic PU matrices.

The CNC/HPU nanocomposite melt-spun fibers exhibited a high degree of CNC alignment and well-aligned HPU polymer chains whose alignment improved with increasing CNC concentration. This is in contrast to an earlier study of nanocomposite fibers using the same CNCs but a hydrophobic PU as matrix, where the CNCs only showed a moderate alignment while the matrix polymer alignment even deteriorated as the CNC load increased.[12] The higher degree of alignment of both CNCs and matrix chains in the HPU-based nanocomposite introduced here indicates that a hydrophilic polymer matrix enables efficient interactions with CNCs.

CNC/HPU nanocomposite fibers showed a significant increase in Young's Modulus with increasing CNC concentration following the predictions of the Halpin–Tsai reinforcement model for unidirectionally aligned CNCs indicating efficient CNC-HPU interactions and a homogeneous dispersion of aligned CNCs within the hydrophilic matrix. These benefits of

ADVANCED
SCIENCE NEWS
www.advancedsciencenews.com

ADVANCED
MATERIALS
INTERFACES
Open Access
www.advmatinterfaces.de

a hydrophilic matrix are directly reflected in the extent of CNC reinforcement in nanocomposite fibers, which is much larger than for hydrophobic PU, with similar stiffnesses at maximum CNC loading despite the three times higher Young's Modulus of the neat hydrophobic PU. Similarly, for the relatively soft HPU matrix used in the present study, the stress-at break increased by nearly a factor of two at high CNC loading, whereas for the stiffer and hydrophobic PU the stress-at-break reduced upon CNC addition.[12]

The results of our study are significant as they illustrate that CNC addition is feasible and beneficial for the melt spinning of nanocomposites containing a hydrophilic and relatively soft matrix phase. While the CNC-reinforcement is lower compared to high aspect-ratio CNCs sourced from prohibitively scarce tunicates,[10] it paves the way for the manufacture of melt-spun CNC/PU nanocomposite based on CNCs from conventional and more abundant sources.

4. Experimental Section

Materials: Whatman Grade 1 filter paper (cotton), anhydrous tetrahydrofuran (THF), phosphoric acid (85 wt%), dimethylformamide (DMF) and ethanol (EtOH), poly(ethylene glycol) (PEG, 1500 g mol^{-1}), poly(propylene glycol) (PPG, 1000 g mol^{-1}), ethylene glycol, and dibutyl tin(II)dilaurate (DBTDL) were purchased from Sigma Aldrich (Buchs, Switzerland). Dicyclohexylmethane-4,4′-diisocyanate (Desmodur W) was purchased from Covestro (Leverkusen, Germany). Deuterated chlorofom (CDCl$_3$) was purchased from Cambridge Isotope Laboratories (Tewksbury, USA). All chemicals were used without further purification.

Synthesis of HPU: The synthesis of hydrophilic polyurethane was carried out under an argon atmosphere using oven-dried glassware. 6 g of PEG (4 mmol, 1 equiv.) were added to a Schlenk flask. The flask was purged with argon by iterating vacuum (shaking vigorously to evacuate air that might be retained by the solid) and argon (3×, starting with vacuum). 1.488 g ethylene glycol (24 mmol, 6 equiv.), 12 g PPG (12 mmol, 3 equiv.) and 100 mL of THF were then added using syringes. The reaction mixture was stirred with a magnetic stirring bar in a water bath at room temperature for 15 min until the PEG had completely dissolved. 38 μL of catalyst DBTDL (64.14 nmol) were mixed in. Then, after 5 min of stirring, 12 g of Desmodur W (45.7 mmol, 12 equiv.) were added and the reaction mixture was stirred for an additional 15 min at ambient temperature before placing it in a pre-heated oil bath at 50 °C. The reaction was carried out at 50 °C for 24 h. The polymer solution was transferred into a hot round bottom flask (250 mL). THF was removed under vacuum and crude PU was post-cured at, unless otherwise noted, 100 °C in a vacuum oven for 24 h. Due to the high mass feed required for extrusion (≈4 g), several batches of hydrophilic PU were synthesized and combined during the preparation of nanocomposite fibers (consistency in the independently synthesized batches was confirmed by standard physical and chemical characterization, see Figures S2–S6, Supporting Information). Gel permeation chromatography (GPC) characterization: PU before post-curing M_w = 22000 g mol^{-1} and Đ = 1.86. PU after post-curing: M_w = 117000 g mol^{-1}, and Đ = 1.46.

Isolation of CNCs: Filter paper was chosen as cellulose source for the CNC extraction; the filter paper was cut into small pieces of ≈1 cm^2 before the hydrolysis. The hydrolysis conditions were adapted from a procedure described by Camarero Espinosa et al.[14] A 75 wt% phosphoric acid solution was prepared by adding 412 mL of 85 wt% phosphoric acid solution to 88 mL of deionized water under vigorous stirring. 15 g of filter paper were added to the acid solution once the acid bath reached 100 °C, followed by stirring for 20 min. Upon completion of the hydrolysis, the solution was cooled down to 25 °C by the addition of 500 g of ice into the solution followed by centrifugation at 14 500 RPM

for 30 min (=20 000 g) the centrifugation step was repeated at least two times until the supernatant was transparent. The remaining suspension was then dialyzed against deionized water for 5 days exchanging the water every day. The final CNC suspension, having a pH of ≈5.5–6.0, was redispersed by sonication for 15 min at 15% amplitude using a Horn ultrasonicator (Branson Digital Sonifer S-250D, 50–60 Hz/200 W). The dispersed suspension was frozen overnight in a freezer and lyophilized in a lyophilizer (Telstar LyoQuest Laboratory Freeze Dryer) for 3 days. The procedure produced CNCs with a 80% yield.

Nanocomposite Fiber Melt Spinning: Nanocomposite fibers containing 0, 5, 10, 15, 20, 22.5, 25 wt% CNCs were prepared using a DACA microcompounder (DACA Instruments, Goleta, US), as previously described.[10] CNC/HPU master batches were prepared to ensure a good dispersion of CNC. For achieving fiber composite of 5, 10, and 15 wt%, 200, 400, and 600 mg of synthesized HPU were mixed with 20 mL DMF and bath-sonicated for a few hours until full dispersion. The CNC solutions were then mixed with 1 g of PU dissolved in 20 mL DMF. Similarly, 20, 22.5, and 25 wt% nanocomposite fibers were prepared by dispersing 800, 900, and 1000 mg of CNCs in 40 mL DMF. Then, 2 g of the synthesized PUs were added to the CNC solutions. Note that different batches of the synthesized PU were combined due to the overall high mass requirements for extrusion. The solutions containing a CNC-PU mixture were stirred overnight, cast into a Teflon Petri dish, followed by an initial oven drying at 50 °C for 3 days, and an additional drying in a vacuum oven at 50 °C for 2 days. Masterbatch films and measured amounts of the synthesized neat PUs were mixed together in the microcompounder to reach concentrations of 0, 5, 10, and 15, 20, 22.5, and 25 wt%. After initial stirring at 100–150 RPM for 5 min at 130 °C, the melt was extruded through a 0.5 mm diameter cylindrical die and then collected on 14 cm diameter rotatory drum in ambient air, which was located at a distance of 10 cm to the extruder. The velocity of the spinning line was adjusted between 50 and 100 RPM to achieve fibers of similar diameters.

Preparation of Solvent-Cast Nanocomposite Films: Nanocomposite films with 5, 10, 15, 20, 22.5, and 25 wt% CNC contents were prepared by solvent casting. 25, 50, 75, 100, 112.5, 125 mg of CNC were dispersed in 20 mL DMF by bath-sonicating the solution for 1 h. 500 mg the synthesized neat PUs were added to the solution and stirred overnight to assure the full dissolution of the polymer. The solutions were then poured into a Teflon Petri dish, oven-dried at 50 °C for 3 days followed by drying in a vacuum oven at 50 °C for 2 days. The resulting films had thicknesses ranging from 70 to 110 μm as determined with a Mitutoyo high-accuracy sub-micron digital micrometer.

HT Model: The Halpin and Tsai model is a semi-empirical model that can be used to predict the mechanical properties of composites reinforced by oriented and non-oriented fibers.[25] The model assumed a homogeneous filler distribution and dispersion, ideal filler–matrix interactions, and no filler–filler interactions. The efficacy of the reinforcement depends on: i) the initial mechanical properties of the matrix and the filler phase, ii) the volume fraction of the filler phase, iii) the aspect ratio of the fillers (assumed identical in shape and size), and iv) the degree of alignment of the fillers. The composite was modeled as a stack of unidirectional plies of various orientations. Depending on the ratio a representing the relative contribution of the longitudinal and transverse components of the Young's modulus, the composite can be modeled either as quasi-isotropic ($E_{c,R}$), aligned along ($E_{c,L}$), or aligned perpendicularly ($E_{c,T}$) to the direction of the applied stress

$$E_{c,L} = \frac{E_m(1 + 2\frac{L}{D}\eta_L\varphi_f)}{(1 - \eta_L\varphi_f)}, \quad \eta_L = \frac{E_f - E_m}{E_f + 2\frac{L}{D}E_m} \tag{1}$$

$$E_{c,T} = \frac{E_m(1 + 2\eta_T\varphi_f)}{(1 - \eta_T\varphi_f)}, \quad \eta_T = \frac{E_f - E_m}{E_f + 2E_m} \tag{2}$$

$$E_{c,R} = a\,E_{c,L} + (1-a)\,E_{c,T} \tag{3}$$

$$a = 0.13 + 0.0815\,\varphi_f - 1.669\frac{E_m}{E_f} \tag{4}$$

where E is Young's modulus, L/D is the aspect ratio of the filler, and φ_f is the volume fraction of the filler phase. The indices m, f, and c refer to the matrix, filler, and composite, respectively. Note that the observed alignment in the matrix polymer (Table 2) is not accounted for in the HT model for aligned fillers, which uses a constant matrix modulus for all filler concentrations. It is important to note, however, that any changes in the modulus due to alignment of the matrix were most likely negligible compared to reinforcement induced by the loading of aligned fillers given their modulus was four orders of magnitude higher (Table 3).

Percolation Model: The percolation model, developed by Takayanagi[26] and Ouali,[27] was first used by Favier et al. to describe the mechanical properties of cellulose/polymer nanocomposite fibers.[28,29] Similar to the aforementioned HT model, the percolation model also assumed a homogeneous filler distribution and dispersion, as well as an ideal filler–matrix interaction. The fillers were, however, assumed to strongly interact with one another, forming a rigid network above a critical filler fraction, denoted as the percolation threshold. The onset of percolation was a function of the fillers aspect ratio as well as their orientation throughout the polymer matrix.[30,31] Below the percolation threshold φ_t, the evolution of the Young's modulus followed a simple series model. Above the percolation threshold, the CNCs assembled into a rigid network, promoted by both Van der Waals forces and hydrogen bonding. The modulus of the composite, E_c, was thus mostly governed by the rigidity of the network, E_n, which differed from the rigidity of an isolated CNC fiber, and by the filler volume fraction

$$E_c = \frac{(1-2\psi+\psi\varphi_f)E_m E_n + (1-\varphi_f)\psi E_n^2}{(1-\varphi_f)E_n + (\varphi_f - \psi)E_m} \tag{5}$$

where the amount of filler ψ that participates in the load transfer is defined as

$$\psi = \begin{cases} 0 & \text{for } \varphi_f \le \varphi_t \\ \varphi_f\left(\dfrac{\varphi_f - \varphi_t}{1-\varphi_t}\right)^b & \text{for } \varphi_f > \varphi_t \end{cases} \tag{6}$$

where, for simplicity, the percolation threshold φ_t is defined assuming an isotropic filler distribution and a fixed aspect ratio[32,33]

$$\varphi_t = \frac{\frac{2L}{D}+\frac{4}{3}}{\frac{32}{3}\left[1+\frac{3}{2}\left(\frac{L}{D}\right)+\frac{3}{8}\left(\frac{L}{D}\right)^2\right]} \tag{7}$$

φ_f is the volume fraction of the filler, $b = 0.4$ is the critical percolation exponent for a 3D percolating network, L/D is the aspect ratio of the CNCs, and E_m, E_n, and E_c are Young's moduli of the matrix, filler, and composite, respectively.

GPC: Experiments were performed on an Agilent 1200 series HPLC system equipped with an Agilent PLgel guard column (particle size: 5.0 μm) and two Aiglent PLgel mixed-D columns (inner diameter: 7.5 mm; length: 300 mm; particle size: 5.0 μm). The signals were recorded by a UV detector (Agilent 1200 series), an Optilab REX interferimetric refractometer, and a miniDawn TREOS light scattering detector (Wyatt Technology Cooperation). The samples were run at 30 °C, by dissolving ≈2 mg of polymer in either THF stabilized with 250 ppm dibuylated hydroxytoluene, or in a DMF solution containing 0.1% w/w LiBr as eluent and a flow rate of 1.0 mL min⁻¹. The data were analyzed using the ASTRA software (Wyatt Technologies Cooperation) and the molecular weights were determined based on a polystyrene calibration curve with molecular weights ranging from 8.844×10^2 to 3.016×10^5 g mol⁻¹.

Nuclear Magnetic Resonance Spectroscopy: Nuclear magnetic resonance (NMR) spectroscopy was carried out at 297.2 K on a Bruker Avance DPX 400 spectrometer (Bruker, Billerica, USA) at a frequency of 400.19 MHz

for ¹H nuclei. The spectra were calibrated to the residual solvent peak of CDCl₃ (7.29 ppm). The data were analyzed with MestReNova (12.0.2) software suite and all chemical shifts δ were reported in part per million (ppm) with coupling constants in Hertz (Hz).

Infrared Spectroscopy: The spectra were recorded using a Spectrometer 65 (Perkin Elmer, Waltham, USA). Samples were measured in ATR mode, while a background spectrum was collected from air. For each measurement, 10 scans with a resolution of 4 cm⁻¹ were averaged. The Spectrum 6 software was used for data analysis.

AFM: AFM imaging of CNCs was performed using a NX10 AFM (Park Systems) operated in tapping mode, using aluminum-coated silicon probes (NanoAndMOre) with a nominal force constant of 40 N m⁻¹, a resonance frequency of 300 kHz, and a tip radius <10 nm. Samples were prepared by depositing 40 μL of an aqueous CNC solution (0.05 mg mL⁻¹) onto freshly cleaved mica followed by drying overnight at room temperature.

TGA: A Mettler–Toledo STAR thermogravimetric analyzer system equipped with Al₂O₃ crucibles was used for thermogravimetric analysis in a temperature range from 0 to 500 °C at a heating rate of 10 °C min⁻¹ under an air atmosphere. Isotherm TGA was conducted similarly by pre-heating the oven chamber to 130 °C followed by inserting the sample and measuring the change of mass during 30 min.

DSC: DSC was conducted on a Mettler Toledo DSC 2 STAR system under nitrogen with a thermal range between 250 and −80 °C. Sample thermal history was leveled by the first thermal cycle, subsequently the second heating cycle is the one exposed in the manuscript. The heating–cooling rate was set to 10 °C min⁻¹.

Tensile Testing: Tensile tests of nanocomposite fibers and films were carried out using a Zwick/Roell Z010 10KN material tensile testing machine. The instrument was equipped with a 200 N load cell and a 2.5 kN clamp for films and with a 5 N load cell and a 20 N clamp for fibers. Fibers were directly mounted and films were cut into dog bone shapes of 5 mm × 22 mm. The samples were tested with a strain-rate of 22 mm min⁻¹ and with a pre-load force of 5 mN.

SEM: The nanocomposite fibers were imaged using a Tescan Mira 3 LMH scanning electron microscope at 4 kV. The fiber nanocomposites samples were rendered conductive by depositing 3 nm of a conductive layer of gold using a 208 HR Cressington sputter coater. The images were processed and analyzed using the ImageJ software.

WAXS: WAXS measurements of nanocomposite samples were performed on a Xeuss 2.0 SAXS/WAXS system (Xenocs) operated at a power of 50 kV/0.6 mA. Monochromatic X-rays having a wavelength of 1.54 Å (Cu Kα radiation) were used to irradiate samples at a sample-to-detector distance of 72 mm, determined by calibration using a silver behenate standard. Exposure times were set to 1 h and scattering patterns were recorded on a Pilatus detector (comprised of three panels) having a total number of pixels of 486 × 618 pixels. The azimuthal profiles were obtained for the [004] and [200] CNC reflections and PU main reflection. To quantify the degree of alignment of CNCs and the PU matrix chains, the azimuthal dependence of each reflection was used to calculate Hermans orientation parameter,[34,35]

$$S = \frac{3\langle\cos^2\phi\rangle - 1}{2} \tag{8}$$

$$\langle\cos^2\phi\rangle = \frac{\int_0^\pi I(\phi)\cos^2\phi\sin\phi\,d\phi}{\int_0^\pi I(\phi)\sin\phi\,d\phi} \tag{9}$$

$I(\phi)$ is the angle-dependent scattering intensity (Figure 5b,c) detected at the azimuthal angle ϕ. $S = 0$ corresponds to isotropic orientation distribution, $S = 1$ corresponds to the complete alignment.

Supporting Information

Supporting Information is available from the Wiley Online Library or from the author.

Conflict of Interest

The authors declare no conflict of interest.

Data Availability Statement

The data supporting the findings of this study are openly available in Zenodo at: https://doi.org/10.5281/zenodo.7543003.

[1] R. J. Moon, A. Martini, J. Nairn, J. Youngblood, A. Martini, J. Nairn, *Chem. Soc. Rev.* **2011**, *40*, 3941.

[2] K. Oksman, Y. Aitomäki, A. P. Mathew, G. Siqueira, Q. Zhou, S. Butylina, S. Tanpichai, X. Zhou, S. Hooshmand, *Composites, Part A* **2016**, *83*, 2.

[3] Y. Habibi, L. A. Lucia, O. J. Rojas, *Chem. Rev.* **2010**, *110*, 3479.

[4] M. Mariano, N. El Kissi, A. Dufresne, *J. Polym. Sci., Part B: Polym. Phys.* **2014**, *52*, 791.

[5] A. Dufresne, *Curr. Opin. Colloid Interface Sci.* **2017**, *29*, 1.

[6] C. M. Clarkson, S. M. El Awad Azrak, E. S. Forti, G. T. Schueneman, R. J. Moon, J. P. Youngblood, *Adv. Mater.* **2021**, *33*, 2000718.

[7] J. O. Akindoyo, M. D. H. Beg, S. Ghazali, M. R. Islam, N. Jeyaratnama, A. R. Yuvaraj, *RSC Adv.* **2016**, *6*, 114453.

[8] M. Khalifa, S. Anandhan, G. Wuzella, H. Lammer, A. R. Mahendran, *Polym.-Plast. Technol. Mater.* **2020**, *59*, 1751.

[9] A. Nicharat, A. Shirole, E. J. Foster, C. Weder, *J. Appl. Polym. Sci.* **2017**, *134*, 1.

[10] A. Redondo, S. Chatterjee, P. Brodard, L. T. J. Korley, C. Weder, I. Gunkel, U. Steiner, *Polymers* **2019**, *11*, 1912.

[11] R. Prataviera, E. Pollet, R. E. S. Bretas, L. Averous, A. de Almeida Lucas, *J. Appl. Polym. Sci.* **2021**, *138*, 50343.

[12] A. Redondo, N. Mortensen, K. Djeghdi, D. Jang, R. D. Ortuso, C. Weder, L. T. J. Korley, U. Steiner, I. Gunkel, *ACS Appl. Mater. Interfaces* **2022**, *14*, 7270.

[13] K. N. M. Amin, N. Amiralian, P. K. Annamalai, G. Edwards, C. Chaleat, D. J. Martin, *Chem. Eng. J.* **2016**, *302*, 406.

[14] S. C. Espinosa, T. Kuhnt, E. J. Foster, C. Weder, *Biomacromolecules* **2013**, *14*, 1223.

[15] J. J. Fallon, B. Q. Kolb, C. J. Herwig, E. J. Foster, M. J. Bortner, *J. Appl. Polym. Sci.* **2019**, *136*, 46992.

[16] M. Mariano, N. El, A. Dufresne, *Eur. Polym. J.* **2015**, *69*, 208.

[17] A. Jalal Uddin, J. Araki, Y. Gotoh, *Biomacromolecules* **2011**, *12*, 617.

[18] W. J. Lee, A. J. Clancy, E. Kontturi, A. Bismarck, M. S. P. Shaffer, *ACS Appl. Mater. Interfaces* **2016**, *8*, 31500.

[19] C. M. Clarkson, S. M. El Awad Azrak, R. Chowdhury, S. N. Shuvo, J. Snyder, G. Schueneman, V. Ortalan, J. P. Youngblood, *ACS Appl. Polym. Mater.* **2018**, *1*, 160.

[20] A. Kiziltas, B. Nazari, E. Erbas Kiziltas, D. J. Gardner, Y. Han, T. S. Rushing, *Carbohydr. Polym.* **2016**, *140*, 393.

[21] C. G. Sig, N. Hakhyun, S. J. Ho, US6509148B2, **2003**.

[22] D. Sakong, M. Cha, J. Shin, G. Cha, M. Ryu, R. Hower, R. Brown, *Sens. Actuators, B* **1996**, *32*, 161.

[23] J. Ho Shin, S. Yong Yoon, I. Jun Yoon, S. Hyuk Choi, S. Dong Lee, H. Nam, G. Sig Cha, *Sens. Actuators, B* **1998**, *50*, 19.

[24] X. Xu, F. Liu, L. Jiang, J. Zhu, D. Haagenson, D. Wiesenborn, *ACS Appl. Mater. Interfaces* **2013**, *5*, 2999.

[25] J. C. Halpin, J. L. Kardos, *J. Appl. Phys.* **1972**, *43*, 2235.

[26] M. Takayanagi, S. Uemura, S. Minami, *J. Polym. Sci., Part C: Polym. Symp.* **1964**, *5*, 113.

[27] N. Ouali, J. Cavaillé, J. Perez, *Plast., Rubber Compos. Process. Appl.* **1991**, *16*, 55.

[28] V. Favier, G. R. Canova, J. Y. Cavaille, H. Chanzy, A. Dufresne, C. Gauthie, *Polym. Adv. Technol.* **1995**, *6*, 351.

[29] V. Favier, G. R. Canova, S. C. Shrivastava, J. Y. Cavaillé, *Polym. Eng. Sci.* **1997**, *37*, 1732.

[30] I. Balberg, N. Binenbaum, N. Wagner, *Phys. Rev. Lett.* **1984**, *52*, 1465.

[31] N. Ueda, M. Taya, *J. Appl. Phys.* **1986**, *60*, 459.

[32] Y. Zare, K. Y. Rhee, *J. Colloid Interface Sci.* **2017**, *506*, 283.

[33] L. Berhan, A. Sastry, *Phys. Rev. E* **2007**, *75*, 041120.

[34] R. A. Chowdhury, S. X. Peng, J. Youngblood, *Cellulose* **2017**, *24*, 1957.

[35] L. Wang, M. Ago, M. Borghei, A. Ishaq, A. C. Papageorgiou, M. Lundahl, O. J. Rojas, *ACS Sustainable Chem. Eng.* **2019**, *7*, 6013.